https://doi.org/10.5194/egusphere-2026-5642
Preprint. Discussion started: 25 September 2026

The Role of Particle Size Distribution in Simulating Aerosol Transport, Radiative Effects and Surface Area of the 2019/20 Australian pyroCb Plume

Sampa Das[1,2], Peter R. Colarco[1], Parker Case[1,2,a], Stephen Steenrod[3], Luke D. Oman[1], and Ghassan Taha[4,1]

[1]Atmospheric Chemistry and Dynamics Laboratory, NASA Goddard Space Flight Center, Greenbelt, Maryland, USA
[2]Earth System Science Interdisciplinary Center, University of Maryland, College Park, Maryland, USA
[3]University of Maryland, Baltimore County, Maryland, USA (retired)
[4]Morgan State University, Baltimore, Maryland, USA
[a] Now at: Rhodium Group, Washington, D.C., USA

Correspondence to: sampa.das@nasa.gov (sdas2021@umd.edu)

Abstract. The 2019/2020 Australian New Year (ANY) pyrocumulonimbus (pyroCb) events injected massive quantities of smoke into the stratosphere, significantly altering Earth's radiative balance and chemical composition. Accurately simulating these impacts in Earth System Models (ESMs) remains challenging, partly because standard bulk aerosol schemes assume particle properties based on tropospheric smoke. In this study, we leverage the NASA GEOS model coupled with the CARMA sectional microphysics module to simulate the rapid microphysical evolution of the ANY pyroCb plume. Our sectional aerosol model simulations reveal that extreme initial number densities drive rapid coagulation, producing stabilized aged particles with an effective radius (R_{eff}) of ~ 0.30 µm, consistent with in-situ and lidar observations. Based on these results and offline Mie-theory calculations, we derive an observationally constrained configuration (R_{eff} = 0.30 µm, σ= 1.2, with moderated near-UV absorption) for the computationally efficient GOCART-2G bulk aerosol module. Compared to the finer-mode baseline, the updated configuration significantly improves simulated aerosol extinction and Ångström Exponent, bringing the plume's spatial distribution and longevity into closer agreement with SAGE-III/ISS and OMPS-LP satellite records. Furthermore, pairing the larger particle size with observationally constrained absorption moderates excessive shortwave radiative heating, enabling more realistic large-scale transport. The larger particle size assumption also reduces the available aerosol Surface Area Density (SAD) by more than a factor of three. Our findings highlight a critical sensitivity to particle size assumptions in simulating large pyroCb events, demonstrating that constraining this property is essential for accurately assessing the plume's radiative impact and its role in heterogeneous chemistry.

1 Introduction

Wildfires emit vast quantities of aerosols and trace gases into the troposphere, heavily influencing regional air quality and radiation budgets. Under extreme meteorological conditions, the intense sensible and latent heat released by these fires can

https://doi.org/10.5194/egusphere-2026-5642
Preprint. Discussion started: 25 September 2026

trigger deep, fire-driven convection known as pyrocumulonimbus (pyroCb). These convective updrafts act as atmospheric chimneys, bypassing the typical tropospheric removal processes and injecting massive quantities of smoke and gaseous precursors directly into the upper troposphere and lower stratosphere (UTLS) (Fromm et al., 2010; Peterson et al., 2018). Once in the stratosphere, where scavenging processes are minimal, these aerosols can reside for months to years, significantly altering the stratospheric radiative balance, circulation, and chemical composition.

The 2019/2020 Australian "Black Summer" fire season culminated in an unprecedented outbreak of pyroCb activity. Between late December 2019 and early January 2020, the Australian New Year (ANY) pyroCb events injected an estimated 0.4 to 1.0 Tg of aerosol mass— alongside massive quantities of water vapor and trace gases such as carbon monoxide (CO) and volatile organic compounds— directly into the stratosphere, dramatically altering its chemical composition (Khaykin et al., 2020; Peterson et al., 2021; Schwartz et al., 2020). This event represents the largest single wildfire-driven perturbation to the stratosphere recorded to date, rivaling the stratospheric aerosol loading of moderate volcanic eruptions. Consequently, the massive aerosol layer significantly altered the Earth's energy budget; observational and modeling estimates indicate a global top-of-atmosphere radiative forcing between -0.4 and -1.0 W m^{-2} in the months following the event, producing a detectable surface cooling effect (Khaykin et al., 2020; Sellitto et al., 2023; Yu et al., 2021). Furthermore, the ANY plume exhibited remarkable dynamic and chemical behavior. Fueled by strong absorption of incoming solar radiation by black and brown carbon, the smoke generated intense localized diabatic heating. This led to dramatic "self-lofting," with distinct smoke vortices ascending deep into the stratosphere (above 30 km) and circumnavigating the globe over several months (Kablick et al., 2020; Ohneiser et al., 2022; Yu et al., 2021). In the months following the injections, the large magnitude of this aerosol loading and surface area further drove observable changes to stratospheric composition, most notably triggering an unprecedented and unexpected repartitioning of mid-latitude stratospheric inorganic chlorine and subsequent stratospheric ozone loss, likely via smoke-driven heterogeneous chemistry (Santee et al., 2022; Solomon et al., 2022, 2023; Strahan et al., 2022).

Accurately representing the transport and climatic impacts of such massive stratospheric injections in global Earth System Models (ESMs) remains a persistent challenge. A major source of this difficulty stems from the assumed microphysical and optical properties of the smoke. Global bulk aerosol models typically parameterize biomass burning aerosols based on observations of standard tropospheric plumes, assuming a relatively small and non-evolving particle size distribution (PSD). However, recent in situ and remote sensing observations reveal that stratospheric pyroCb aerosols are microphysically distinct. Measurements from field campaigns, such as ATom (Atmospheric Tomography Mission) and DCOTSS (Dynamics and Chemistry of the Summer Stratosphere), alongside multi-wavelength lidar inversions, indicate that mature pyroCb plumes are composed of significantly larger particles (effective radii ~ 0.2 to 0.3 μm) than typical tropospheric smoke (Katich et al., 2023; Li et al., 2025; Murphy et al., 2021; Ohneiser et al., 2022). Furthermore, these observations frequently reveal complex mixing states, such as black carbon cores enveloped by thick organic and sulfate coatings, which can substantially alter the aerosols' scattering and absorption efficiencies. While explicitly resolving these intricate fractal morphologies and core-shell optics remains computationally prohibitive in standard global bulk aerosol modules, correcting the fundamental baseline assumptions

https://doi.org/10.5194/egusphere-2026-5642
Preprint. Discussion started: 25 September 2026

regarding the particle size distribution is a critical and achievable first step. Because a particle's bulk size and variance dictate its scattering efficiency, absorption potential, and available surface area, relying on standard tropospheric assumptions critically undermines a global model's ability to simulate realistic radiative heating rates and chemical reactivity.

To address this gap, this study investigates the microphysical evolution of the ANY pyroCb plume and derives observationally constrained aerosol optical assumptions for global climate modeling. We leverage CARMA (the Community Aerosol and Radiation Model for Atmospheres), a sectional microphysics module coupled within the NASA GEOS (Goddard Earth Observing System) framework (Case et al., 2023, 2024; Colarco et al., 2014), to explicitly simulate the rapid growth and aging of the stratospheric smoke. Using these sectional results and offline Mie theory calculations, we subsequently design a modified configuration for the computationally efficient GOCART-2G (Goddard Chemistry Aerosol Radiation and Transport model, Collow et al., 2024) bulk aerosol module. By comparing the baseline and modified bulk configurations, we explore how proper particle size distribution assumptions control the simulated radiative forcing, large-scale transport, and the total aerosol surface area available for heterogeneous chemistry.

The remainder of this manuscript is organized as follows: Section 2 details the GEOS model configuration, the CARMA and GOCART-2G aerosol modules, the injection parameters utilized for the ANY event, and the satellite observational datasets (SAGE-III and OMPS-LP) used for evaluation. Section 3 presents the results, beginning with the simulated microphysical evolution of the plume and the derivation of the updated pyroCb optics. This is followed by validation of the simulated optical properties and spatial transport against satellite observations, and an analysis of the resulting impacts on shortwave radiative heating and surface area density (SAD). Finally, Sect. 4 provides a summary and conclusions, outlining how these microphysical constraints set the necessary foundation for a subsequent study exploring the role of heterogenous chemistry and particle composition in stratospheric ozone depletion associated with pyroCb emitted smoke plumes.

2 Approach and Methods

2.1 Model Description and Configuration

The GEOS ESM integrates components for atmospheric and oceanic circulation, land-surface processes, land- and sea-ice, and ocean biogeochemistry, supported by a robust atmospheric data assimilation framework (Molod et al., 2015; Rienecker et al., 2008). GEOS ESM employs a finite-volume dynamical core on a cubed-sphere grid (Putman and Lin, 2007; Putman and Suarez, 2011) and incorporates comprehensive physical parameterizations for convection, large-scale precipitation and cloud cover, longwave and shortwave radiation, turbulence and boundary layer mixing, and gravity wave drag. The model offers several chemistry and aerosol mechanisms to simulate atmospheric composition. This study focuses on two aerosol modules:

(1) **GOCART-2G** (Collow et al., 2024) represents a refactored and updated version of GOCART (Chin et al., 2002; Colarco et al., 2010). This bulk scheme simulates the sources and sinks of dust, sea salt, sulfate, nitrate, black carbon (BC), and organic aerosols (OA). GOCART-2G introduces brown carbon (BR) components following Colarco et al. (2017) and

https://doi.org/10.5194/egusphere-2026-5642
Preprint. Discussion started: 25 September 2026

implements a simplified secondary organic aerosol (SOA) mechanism (Hodzic and Jimenez, 2011; Kim et al., 2015). Importantly for this study, GOCART-2G (also occasionally referred to as GOCART) tracks aerosol mass for individual species, but the PSD for each species remains static and does not evolve with smoke age.

(2) **CARMA** is based on a sectional aerosol microphysics scheme that enables aerosols to grow across size bins, shrink, and undergo removal through microphysical processes including coagulation, condensation, evaporation, and gravitational settling (Toon et al., 1988). Colarco et al. (2014) initially implemented CARMA into GEOS, while Case et al. (2023, 2024) enhanced its stratospheric capabilities by coupling aerosol mechanisms with full gas-phase chemistry in GEOS.

The standard GEOS ESM configuration operates online with the GOCART-2G aerosol module due to its superior computational efficiency. In this study, we leverage CARMA's detailed microphysics to investigate particle growth mechanisms and develop improved PSD assumptions for GOCART-2G that better represent pyroCb-emitted smoke particles. We apply identical injection parameters (Peterson et al., 2021; Yu et al., 2021) for the ANY pyroCb case (Table 1) to both CARMA and GOCART-2G and conduct two sets of simulations with radiative coupling to GEOS ESM.

Table 1. List of injection parameters to simulate ANY 2020 pyroCb events within GEOS c90 resolution.

Injection Parameters	Values
Injected smoke mass*	0.9 Tg smoke mass
Injection Height	12-13 km
Injection days	December 2019: 29, 30, 31 of 2019 and January 4 of 2020, for 5 hours each day
Injection Location	39°S, 150°E

* The injected smoke mass in CARMA is treated entirely as Organic Carbon (OC), whereas the GOCART-2G module partitions the mass into 98% Brown Carbon (BR)— which has similar microphysical properties to OC— and 2% Black Carbon (BC).

Figure 1 presents the initial PSD assumptions for both CARMA and the baseline GOCART-2G simulations, overlaying the lognormal particle number size distribution that best fits measurements from ORACLES (ObseRvations of Aerosols above CLouds and their intEractionS; Redemann et al. (2021)) and ATom field campaigns of tropospheric smoke cases. The measured aerosol PSD aligns well with CARMA's assumed initial PSD, while by default GOCART-2G assumes significantly smaller particles following Chin et al. (2002).

https://doi.org/10.5194/egusphere-2026-5642
Preprint. Discussion started: 25 September 2026

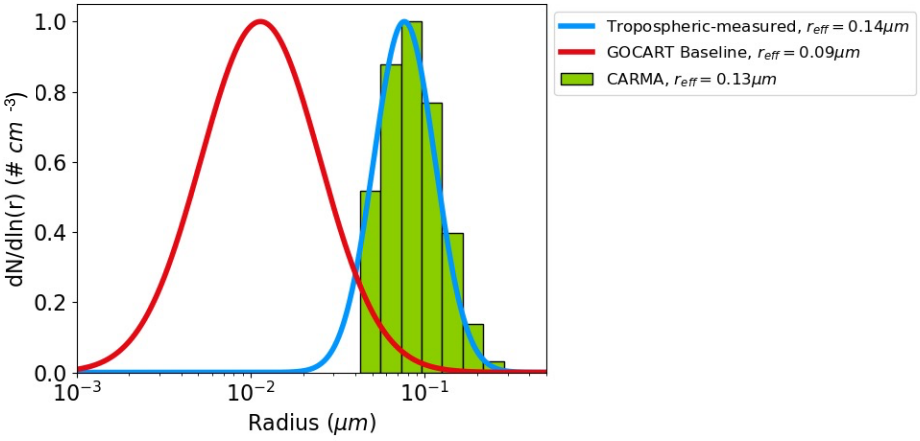

Figure 1: Initial number particle size distribution (PSD) assumptions for CARMA (green bars), baseline GOCART-2G(red) and measured during ORACLES and ATom campaign (blue).

All simulations run at c90 (~1-degree) horizontal resolution with 72 vertical hybrid sigma levels extending from the surface to ~80 km altitude. The model is replayed to assimilated meteorological fields produced by the near-real time GEOS-FP (https://gmao.gsfc.nasa.gov/weather-analysis-prediction/, version f522) system to constrain it with realistic meteorology. It should be noted that vertical evolution of pyroCb plumes in the stratosphere following point injections is very sensitive to injection parameters, choice of horizontal resolution, as well as mode of simulation (i.e., replay versus free-running). Injection parameters were iteratively varied until comparable match to satellite-observed aerosol distribution was achieved.

2.2 Observational Datasets

To rigorously evaluate the simulated aerosol optical properties, vertical distribution, and transport of the ANY pyroCb plumes, this study leverages spaceborne observations from two complementary satellite instruments: the Stratospheric Aerosol and Gas Experiment III on the International Space Station (SAGE-III/ISS) and the Ozone Mapping and Profiler Suite-Limb Profiler (OMPS-LP) onboard Suomi-NPP.

2.2.1 SAGE-III

SAGE-III/ISS utilizes the solar occultation technique to measure vertical profiles of aerosol extinction, ozone, and other trace gases (Cisewski et al., 2014). Because solar occultation relies on directly viewing the sun through the Earth's limb, it provides exceptionally high vertical resolution (~0.75 km, reported every 0.5 km) and high-precision extinction measurements across a broad spectral range. The SAGE III/ISS aerosol retrieval algorithm is essentially the same as its predecessor on the Meteor 3M platform (Thomason et al., 2010; Thomason and Taha, 2003). In this study, we utilize the SAGE-III version 5.3 level 2 aerosol extinction data. Specifically, we extract extinction coefficients at the 521 nm and 1022 nm channels to evaluate the model's simulated extinction and to calculate the observational Ångström Exponent (AE). The multi-wavelength AE serves as

https://doi.org/10.5194/egusphere-2026-5642
Preprint. Discussion started: 25 September 2026

a critical observational proxy for validating the simulated particle size distributions. It should be noted that while SAGE-III provides highly accurate profiles, the long line-of-sight in the limb occultation geometry is prone to signal saturation and total attenuation in optically thick environments (Khaykin et al., 2020; Taha et al., 2021). Consequently, retrievals immediately following the massive ANY injections are often muted or missing, requiring the manual identification of unsaturated smoke profiles for proper microphysical evaluation.

2.2.2 OMPS-LP

We use the OMPS-LP onboard the Suomi National Polar-orbiting Partnership (Suomi-NPP) satellite (Flynn et al., 2014). OMPS-LP measures solar radiances scattered from the Earth's atmospheric limb. Unlike the sparse spatial sampling afforded by solar occultation measurements, this limb-scattering technique uses three vertical slits separated horizontally to provide near-global coverage in 3–4 days. This high temporal and spatial resolution make OMPS-LP exceptionally well-suited for tracking the evolution, vertical lofting, and latitudinal spread of stratospheric aerosol plumes over time. In this study, we utilize the OMPS-LP version 2.5 aerosol extinction retrieval product (Taha et al., 2021) at the 869 nm wavelength, which is then gridded at a 1.5° latitude by 20° longitude horizontal resolution at a daily interval. The vertical resolution of the extinction product is ~1.6 km (reported every 1 km), extending from 10 to 40 km above sea level. We used cloud-unfiltered data to ensure that potential biomass and volcanic aerosol signals near the tropopause remain apparent in the dataset. Measurements at or below the tropopause are, however, often affected by actual cloud contamination.

3 Results and Discussions

3.1 Initial Plume Evolution and Discrepancies in Aerosol Extinction

To evaluate our simulation of the immediate aftermath of the ANY pyroCb injections (spanning December 29–31, 2019, and January 4, 2020), we examine the zonal mean aerosol extinction profiles in the lower stratosphere. Figure 2 compares the spatial distribution and vertical spread of the plume as observed by the OMPS-Limb Profiler (OMPS-LP) against simulations from CARMA and the baseline GOCART-2G module during two consecutive 10-day periods following the initial injections.

https://doi.org/10.5194/egusphere-2026-5642
Preprint. Discussion started: 25 September 2026

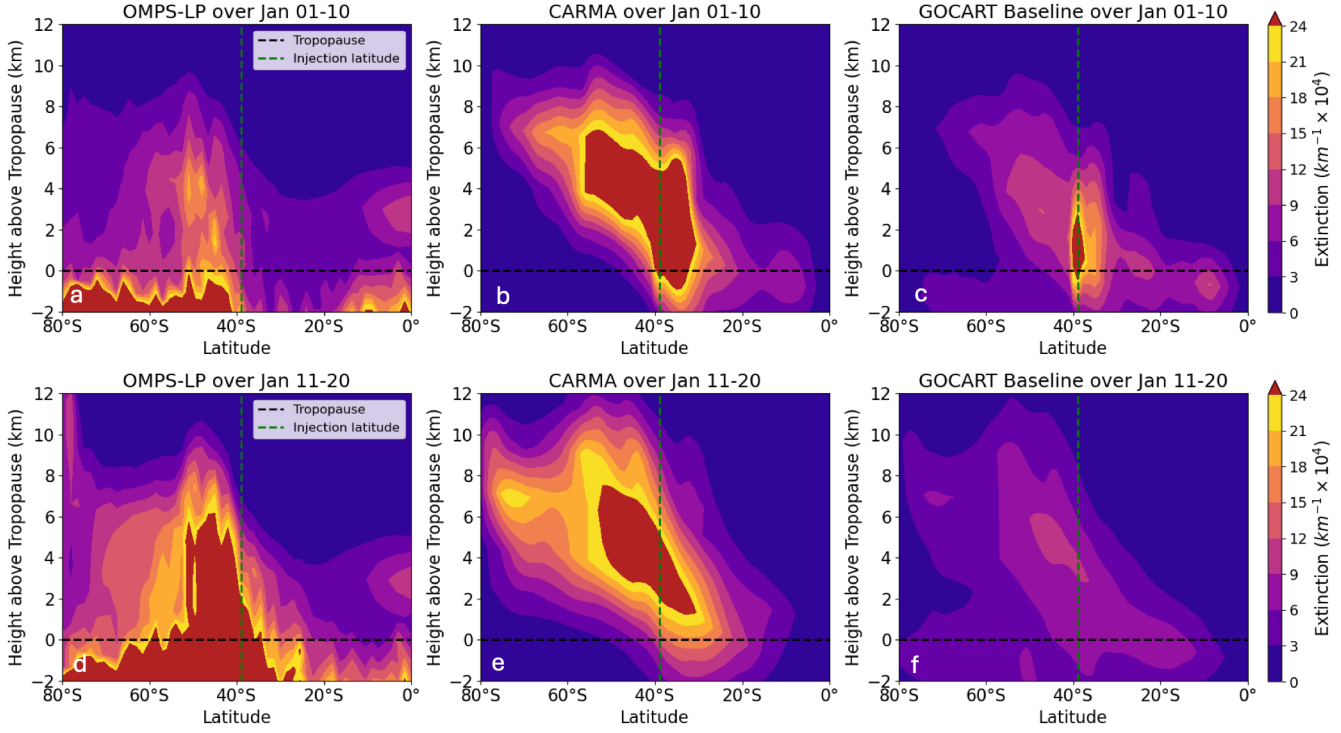

Figure 2. Zonal mean aerosol extinction ($km^{-1} \times 10^4$) at 870 nm during the first 20 days following the ANY pyroCb injections, plotted as a function of height above the tropopause. The top row shows the period of January 1–10, 2020, for (a) OMPS-LP observations, (b) CARMA, and (c) the baseline GOCART configuration. The bottom row shows the subsequent period of January 11–20, 2020, for (d) OMPS-LP, (e) CARMA, and (f) baseline GOCART. The horizontal dashed black line at 0 km denotes the local tropopause height. The vertical dashed green line indicates the injection latitude (39°S).

The observations and simulations both show enhanced stratospheric aerosol that rapidly transports south of the injection latitude. Direct quantitative comparisons with OMPS-LP retrievals (Fig. 2a) are challenging during the earliest period (January 1–10). In the days immediately following the pyroCb injections, the intense optical thickness of the plume saturates the optical path length for the limb profiler, resulting in muted retrieved extinctions that do not fully capture the peak plume intensity within the stratosphere. Furthermore, the exceptionally high extinctions observed at and below the tropopause in the OMPS-LP data are affected by cloud contamination. Since we utilized cloud-unfiltered retrievals to preserve the dense smoke signal, the retrieval algorithm cannot completely distinguish between the pyroCb aerosols and upper-tropospheric clouds. However, this is not an issue here since the focus of this analysis is the relative difference between the two aerosol modules within the stratosphere.

Despite utilizing identical injection parameters and total injected mass (0.9 Tg), the different aerosol modules simulate markedly different plume evolutions. Within the first 10 days (Figs. 2b and 2c), the baseline GOCART-2G simulation produces noticeably lower extinction magnitudes than CARMA. As the plume ages into the subsequent 10-day period (January 11–20, Fig. 2d–f), it spreads both vertically and horizontally. This spatial dispersion and subsequent dilution reduce the optical

https://doi.org/10.5194/egusphere-2026-5642
Preprint. Discussion started: 25 September 2026

thickness sufficiently for OMPS-LP to capture a much stronger and more representative signal of the ANY injections (Fig. 2d). During this timeframe, while the CARMA simulation maintains robust extinction magnitudes that are comparable in magnitude and spatial structure to the OMPS-LP observations (Fig. 2e), the baseline GOCART-2G extinction magnitudes are severely underestimated compared to both CARMA and OMPS-LP (Fig. 2f).

Furthermore, slight but important divergences in transport and vertical spread begin to emerge between the two simulations. During the initial evolution period (January 1–10), the baseline GOCART simulation exhibits a preferential transport north of the injection latitude (equatorward). In contrast, the CARMA plume exhibits a distinct southward (poleward) preference that more closely aligns with the spatial structure of the OMPS-LP observations. This divergence in early horizontal transport between the two modules can be attributed to differences in aerosol radiative forcing and subsequent diabatic self-lofting.

Given these stark contrasts in simulated extinction, it is necessary to determine the underlying cause. The physical relationship governing aerosol extinction at a given wavelength (λ) and relative humidity (RH) can be expressed as:

$$\text{Extinction}\,(RH,\lambda) = [\text{Aerosol Mass}] \times f(RH) \times \text{MEE}, \quad (1)$$

where [Aerosol Mass] is the simulated mass concentration, $f(RH)$ is the scattering enhancement factor (a measure of hygroscopic growth), and MEE is the Mass Extinction Efficiency. The MEE itself is intrinsically linked to the aerosol microphysics, functioning as a dependent variable of the particle effective size and the complex refractive index.

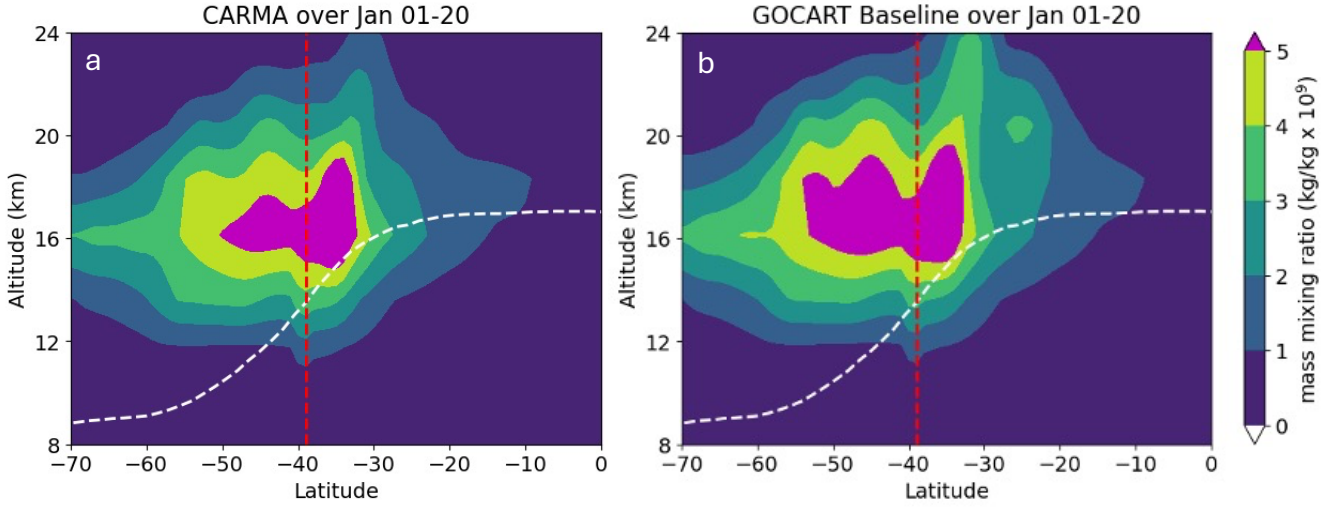

Figure 3. Zonal mean aerosol mass mixing ratio (kg/kg × 10^9) averaged over the first 20 days following the ANY pyroCb injections (January 1–20, 2020) for (a) CARMA and (b) the baseline GOCART-2G simulation. The dashed white line denotes the tropopause height, and the vertical dashed red line indicates the injection latitude (39°S).

To isolate the variables governing the simulated extinction, Fig. 3 presents the zonal mean aerosol mass mixing ratio averaged over the entire initial evolution period (January 1–20) for both CARMA and the baseline GOCART-2G simulations. It is important to note a minor compositional difference in how the injected mass is treated between the two configurations. At the

https://doi.org/10.5194/egusphere-2026-5642
Preprint. Discussion started: 25 September 2026

time of this study, the version of CARMA coupled within GEOS was limited to handling a single aerosol species at a time; consequently, the injected smoke mass in CARMA is treated entirely as Organic Carbon (OC). In contrast, the baseline GOCART-2G module allows for multi-species partitioning, treating the injected mass as 98% Brown Carbon (BR)—which has similar bulk physical properties to OC—and 2% Black Carbon (BC). Despite this difference in speciation, the spatial distribution and cumulative mass prevailing above the tropopause are similar between the two modules over the January 1–20 period. In fact, the total simulated aerosol mass in the lower stratosphere is slightly larger and extends further vertically in the baseline GOCART-2G simulation (Fig. 3b) than in CARMA (Fig. 3a).

Returning to our extinction relationship (Eq. 1), the baseline GOCART-2G model simulates slightly greater stratospheric aerosol mass and vertical extent compared to CARMA yet produces significantly lower aerosol extinction over this same 20-day period (as shown in Fig. 2). Because both simulations are constrained by the same replayed meteorology and relative humidity fields, this discrepancy indicates the MEE in the baseline GOCART-2G configuration is substantially lower than that of CARMA. Since MEE is a direct function of the aerosol size, this definitively confirms that GOCART-2G's non-evolving PSD assumption (Fig. 1) is inadequate for capturing the optical properties of the aging pyroCb plume.

3.2 Evolution of the Particle Size Distribution (PSD)

Having established that differences in the Mass Extinction Efficiency (MEE) are the primary drivers of the extinction discrepancies between the two aerosol modules, we now examine the microphysical evolution simulated by CARMA. Figure 4 illustrates the temporal evolution of effective radius (R_{eff}), MEE, and peak aerosol extinction within the CARMA-simulated ANY smoke plume at the ~18 km altitude level. To explicitly track the densest portion of the plume before it homogeneously spreads across the mid-latitudes, values are extracted from the specific grid cell exhibiting the maximum stratospheric extinction at each timestep and altitude.

https://doi.org/10.5194/egusphere-2026-5642
Preprint. Discussion started: 25 September 2026

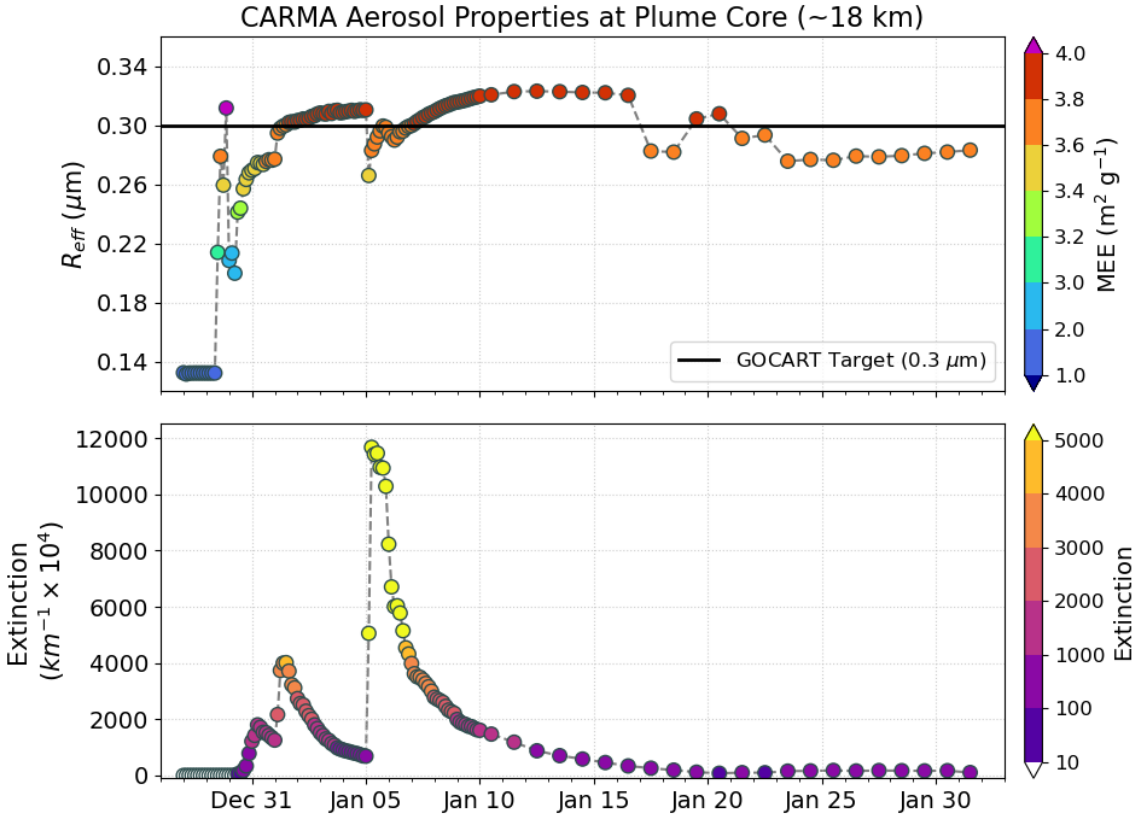

Figure 4. Microphysical and optical evolution of the CARMA-simulated ANY pyroCb plume core at ~18 km. Values represent the grid cell with maximum extinction at each timestep. (a) Effective radius (R_{eff}, μm) colored by corresponding Mass Extinction Efficiency (MEE, m² g⁻¹ at 870 nm), with the solid black line denoting the 0.3 μm target utilized for the updated GOCART configuration. (b) Peak aerosol extinction (km⁻¹ × 10⁴). The timeseries uses 3-hourly resolution during the initial injections and rapid coagulation phase, transitioning to daily resolution as the mature plume stabilizes.

Upon injection, the CARMA aerosol size distribution is initialized with an effective radius of 0.13 μm (Fig. 1). However, extreme particle number densities within the highly concentrated fresh plume facilitate rapid microphysical processing by coagulation. As shown in Fig. 4a, R_{eff} increases significantly within the first few days. The episodic nature of the modelled injections is clearly visible during this early phase. Massive influxes of fresh, fine-mode smoke cause temporary reductions in the mean particle size. This is most notable during the largest injection on January 4 (indicated by the sharp extinction spike in Fig. 4b), though the reduction is quickly overcome as robust coagulation resumes.

This microphysical evolution, however, also exhibits a distinct vertical gradient due to the combined effects of episodic fresh injections, coagulation, and size-dependent sedimentation. As shown in Fig. S1, the lower 16 km altitude level is physically closer to the initial injection height (of ~12 km) and thus experiences sooner and more frequent influxes of fresh smoke compared to 18 km, alongside the continuous sedimentation of larger particles from above. This results in a highly variable

https://doi.org/10.5194/egusphere-2026-5642
Preprint. Discussion started: 25 September 2026

early growth trajectory. Despite this initial variability, the particle size distribution across the bulk of the stratospheric smoke layer (16–18 km) ultimately reaches a stabilized state by late January, wherein particles cease to grow further, with both altitude levels asymptote towards an effective radius of 0.30 µm (Figs. 4a and S1a). This is strongly supported by independent observations, including multiwavelength lidar inversions deriving R_{eff} = 0.29 µm for the ANY aged smoke (Ohneiser et al., 2022), and in situ measurements from the DCOTSS and ATom campaigns (Reff ~0.25 µm) (Chen et al., 2026; Katich et al., 2023; Li et al., 2025). Consequently, as the particles grow, the optical properties of the smoke shift, as demonstrated by the color mapping in Fig. 4a, the MEE steeply increases from roughly 1.0 m^2 g^{-1} at injection to stable values of 3.6 to 3.8 m^2 g^{-1}.

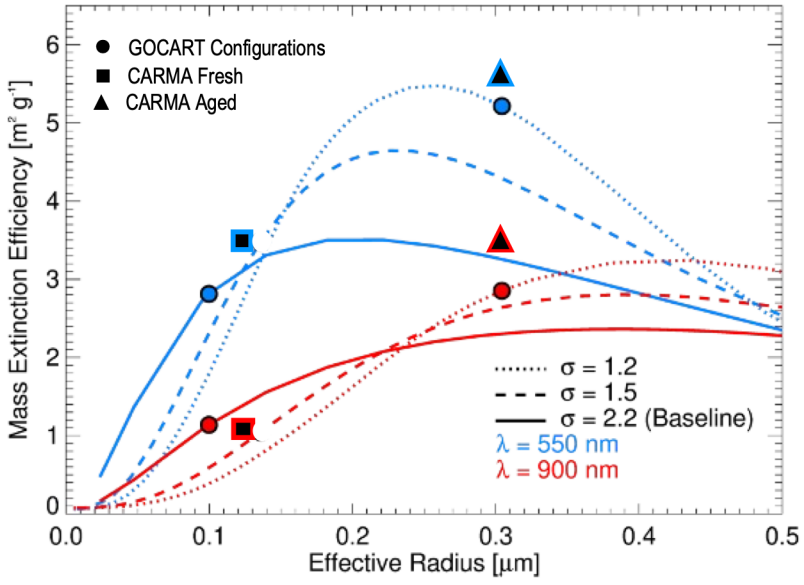

Figure 5. Offline Mie-theory calculations of Mass Extinction Efficiency (MEE) for organic aerosols as a function of effective radius (Reff) and geometric standard deviation (σ). Theoretical curves are shown for 550 nm (blue) and 900 nm (red) wavelengths at varying distribution widths (solid lines: σ = 2.2; dashed lines: σ = 1.5; dotted lines: σ = 1.2). Open squares and triangles denote the MEE of the fresh and aged CARMA plumes, respectively. Solid circles indicate the specific configurations utilized in the GOCART module: the baseline configuration (Reff = 0.09 µm, mapped on the solid curves) and the updated pyroCb PSD/optics configuration (Reff = 0.3 µm, mapped on the dotted curves).

To translate these sectional microphysical findings into a framework compatible with GOCART-2G's bulk lognormal parameterization, we conducted offline Mie theory calculations for organic aerosols (Fig. 5). These calculations evaluate how MEE responds to changes in both effective radius (R_{eff}) and the geometric standard deviation (σ) of the lognormal size distribution at visible (550 nm) and near-infrared (900 nm) wavelengths. The baseline GOCART-2G assumption employs a broad distribution (σ = 2.2, solid lines). As Fig. 5 demonstrates, simply increasing the R_{eff} within this broad baseline distribution is insufficient to reproduce the high MEE values achieved by the aged CARMA plume. Instead, matching the optical properties

https://doi.org/10.5194/egusphere-2026-5642
Preprint. Discussion started: 25 September 2026

of the aged CARMA smoke (black triangles) requires not only a larger effective radius but also a narrower size distribution. The offline calculations show that a lognormal distribution with $R_{eff} \approx 0.30$ µm and a narrowed geometric standard deviation of $\sigma = 1.2$ (dotted lines) excellently reproduces the target CARMA MEE at both 550 nm and 900 nm. However, it is also important to note that the higher MEE associated with this larger R_{eff} inherently increases the absorption coefficient and the bulk absorption of the plume. Therefore, to prevent the model from overestimating the aerosol absorption potential due to this size increase, we scaled down the absorption for organic aerosols (OA) in the near-UV. This adjustment is based on findings from Single Scattering Albedo (SSA) and Lidar Ratio model-data comparison analysis during the ORACLES field campaign over the south-east Atlantic region (Das et al., 2024). Together, the combination of a larger effective radius ($R_{eff} = 0.3$ µm), a narrower size distribution ($\sigma = 1.2$), and the lowered OA absorption in the near-UV constitutes what we hereafter refer to as the "pyroCb PSD/optics" configuration.

Lastly, it is also important to acknowledge certain caveats inherent to this methodological approach. Our optical calculations assume perfectly spherical and externally mixed aerosols. In reality, biomass burning aerosols can exhibit complex morphologies, such as fractal aggregates of black carbon (Yu et al., 2021), and age into intricate core-shell mixing states (e.g., Chen et al., 2026). However, the exact morphological evolution of pyroCb aerosols in the stratosphere remains highly uncertain. As demonstrated in our prior simulation of the 2017 British Columbia pyroCb events (Das et al., 2021), the observed rate of plume ascent was successfully captured without invoking these highly sophisticated morphological assumptions. Building upon this, we continue to adopt a simplistic approach by assuming a single-mode lognormal distribution of spherical, externally mixed particles, but directly constraining their size and absorption potential based on available observations.

3.3 Evaluation of Aerosol Optical Properties

To evaluate the performance of the newly derived pyroCb PSD/optics configuration, we compare the GEOS simulated aerosol extinction and Ångström Exponent (AE) against independent observational datasets.

https://doi.org/10.5194/egusphere-2026-5642
Preprint. Discussion started: 25 September 2026

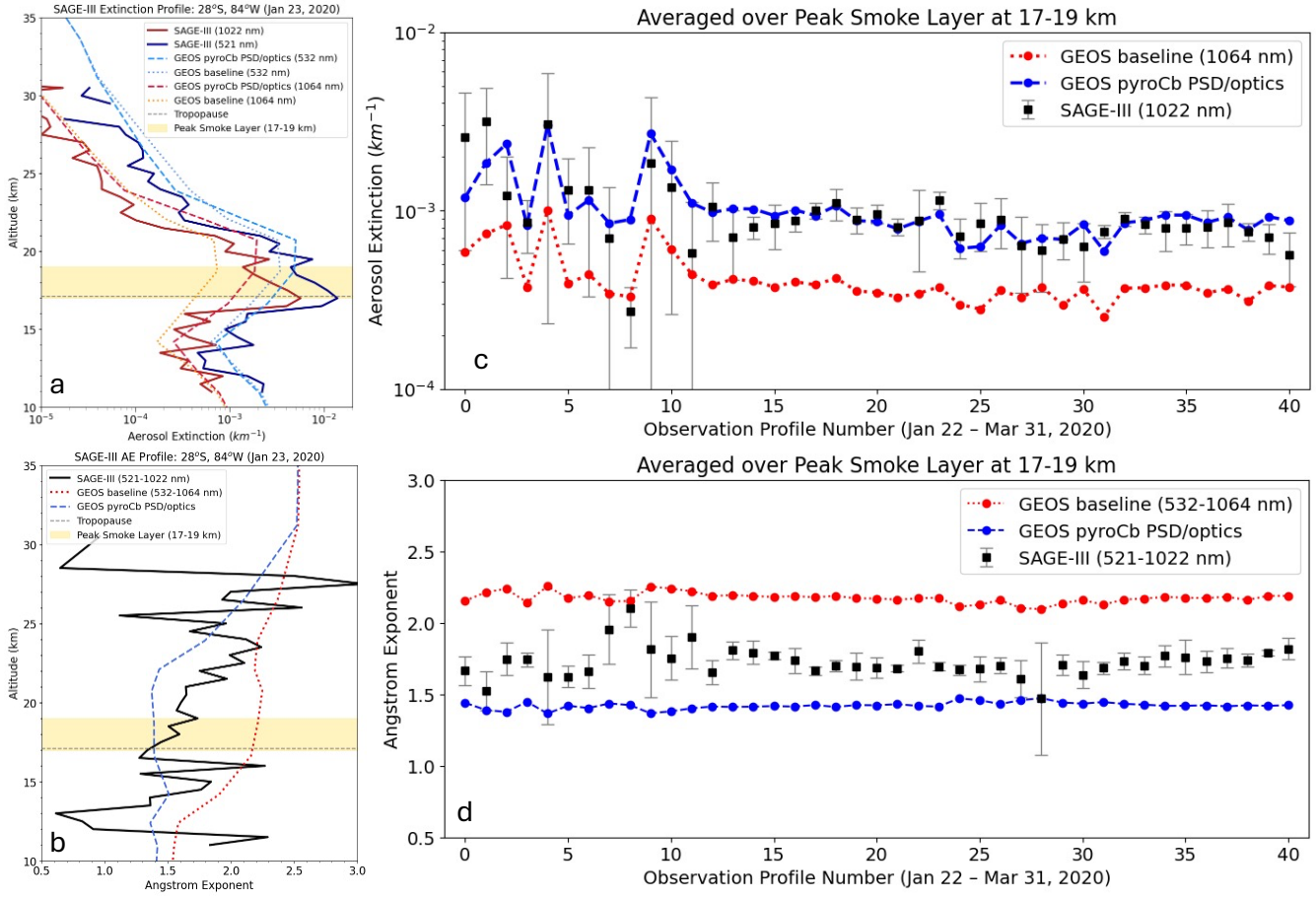

Figure 6. Comparison of GEOS simulated aerosol properties against SAGE-III/ISS solar occultation measurements. (a) Aerosol extinction and (b) Angstrom Exponent profiles for a single unsaturated profile on January 23, 2020 (28°S, 84°W). The yellow shaded region indicates the peak stratospheric smoke layer (17–19 km). Time series of (c) mean aerosol extinction and (d) mean Ångström Exponent averaged over the 17–19 km smoke layer for 40 individual SAGE-III profiles intercepted between January 22 and March 31, 2020. Dashed blue lines indicate the updated GEOS pyroCb PSD/optics configuration, while dotted red lines represent the baseline GEOS configuration. GEOS simulated optical properties at 532 nm and 1064 nm are compared to SAGE-III/ISS retrievals at 521 nm and 1022 nm, respectively, as the closest available wavelength proxies.

Figure 6 presents a detailed comparison of the model against SAGE-III/ISS solar occultation measurements. It is important to note that solar occultation retrievals, particularly at 521 nm, are often saturated by optically thick plumes in the immediate aftermath of massive pyroCb injections. Consequently, SAGE-III/ISS is unable to capture the very initial microphysical evolution of the size distribution following the injections. The profile shown in Figs. 6a and 6b, captured on January 23, 2020, represents the first cleanly unsaturated profile identified in our timeseries, allowing for a robust evaluation of the simulated optical properties.

As demonstrated in Fig. 6a, the baseline GEOS configuration significantly underestimates the extinction within the main stratospheric smoke layer (highlighted between 17 and 19 km). By implementing the pyroCb PSD/optics, the model captures

https://doi.org/10.5194/egusphere-2026-5642
Preprint. Discussion started: 25 September 2026

both the magnitude of the extinction and the general vertical distribution of the aerosol plume. This improvement is fundamentally driven by the updated particle size assumptions, as corroborated by the AE profiles in Fig. 6b. The SAGE-III/ISS observations show a sharp drop in AE from background stratospheric values (roughly 2.0 to 2.5) down to approximately 1.5 within the plume core. This drop signifies a shift in the stratospheric composition due to the presence of large, aged pyroCb particles in the lower stratosphere as opposed to the smaller background sulphate particles at higher altitudes. The baseline model fails to capture this shift. In contrast, the modified pyroCb PSD/optics configuration closely reproduces the observed AE drop. Furthermore, at altitudes above 25 km, where the atmosphere is mostly dominated by background sulphate aerosols, both the simulated background extinction and AE by the modified configuration closely match SAGE-III observations as well.

To assess the temporal evolution of the plume, Figs. 6c and 6d track the mean extinction and AE within the peak smoke layer (17 to 19 km) across 40 individually identified SAGE-III profiles spanning January 22 to March 31, 2020. These specific profiles were manually isolated to ensure a clear smoke signal, utilizing a combination of extinction and AE thresholds. The time series reveals two distinct phases. The initial phase (roughly the first 10 profiles) exhibits high variability and noise, reflecting the dense, concentrated, and heterogeneous nature of the smoke plumes shortly after injection. After approximately one and a half months (around profile #12), the plumes dilute and spatially spread, transitioning into a stabilized regime.

The GEOS model run with the pyroCb PSD/optics successfully captures both dynamics. It tracks the high variance in extinction during the initial noisy phase and smoothly captures the stabilized extinction magnitudes observed from late February onward (Fig. 6c). Most importantly, as shown in Fig. 6d, the modified optics configuration consistently maintains an AE of ~1.4 to 1.5 throughout the entire three-month period, accurately reflecting the influence of injected smoke within the relatively pristine stratospheric background. The baseline model misses this microphysical reality, erroneously maintaining an AE above 2.1, closer to the background aerosol AE value, throughout the entire period. This microphysical fidelity extends to higher altitudes (26–28 km; Fig. S2). It should be noted that background aerosol concentrations at these altitudes are extremely low, leading to a reduced signal-to-noise ratio in the SAGE-III retrievals and consequently larger uncertainties in observed extinction. While both configurations simulate comparable extinction magnitudes to SAGE-III retrievals above the primary smoke core, only the pyroCb PSD/optics configuration captures the compositional shift driven by gradual diabatic lofting of smoke. As the smoke gradually intrudes into this layer (around profile #12-15), SAGE-III and the updated model both exhibit a distinct decline in AE, reflecting the arrival of larger smoke particles as opposed to maintaining a flat AE near 2.5 like the baseline simulation. Further, the updated configuration reduces the mean AE bias by over 70% (from 0.44 to 0.12) and lowers the mean absolute error (Fig. S2b).

To further validate the spatial and temporal evolution of the plume, we evaluate the simulated aerosol extinction against observations from the OMPS-LP. Figure 7 presents the zonal mean aerosol extinction at 869 nm along the 18.5 km altitude, near the core of the stratospheric smoke layer, spanning from December 2019 through March 2020. The OMPS-LP observations (Fig. 7a) illustrate the massive scale and longevity of the ANY pyroCb event. Following the initial injections at 39°S in late December and early January, the highly scattering smoke plume not only intensifies but also exhibits significant

https://doi.org/10.5194/egusphere-2026-5642
Preprint. Discussion started: 25 September 2026

325 equatorward transport, spreading across the mid-latitudes and persisting at high extinction magnitudes ($> 1.5 \times 10^{-3}$ km^{-1}) well into March.

As shown in Fig. 7b, the baseline GEOS configuration drastically underestimates the magnitude and apparent lifespan of the stratospheric plume at this altitude. This discrepancy is a direct result of the optical limitations of the finer-mode size assumption. Although significant aerosol mass is present at the 18.5 km level in the simulation, the resulting MEE is too low
330 to reproduce the intense optical thickness observed by OMPS-LP. Consequently, the simulated plume remains optically muted, making it appear to prematurely dissipate and fail to capture the observed equatorward spread. In stark contrast, the GEOS simulation utilizing the updated pyroCb PSD/optics (Fig. 7c) successfully captures the spatial distribution, extinction magnitudes, and longevity of the plume as observed by OMPS-LP.

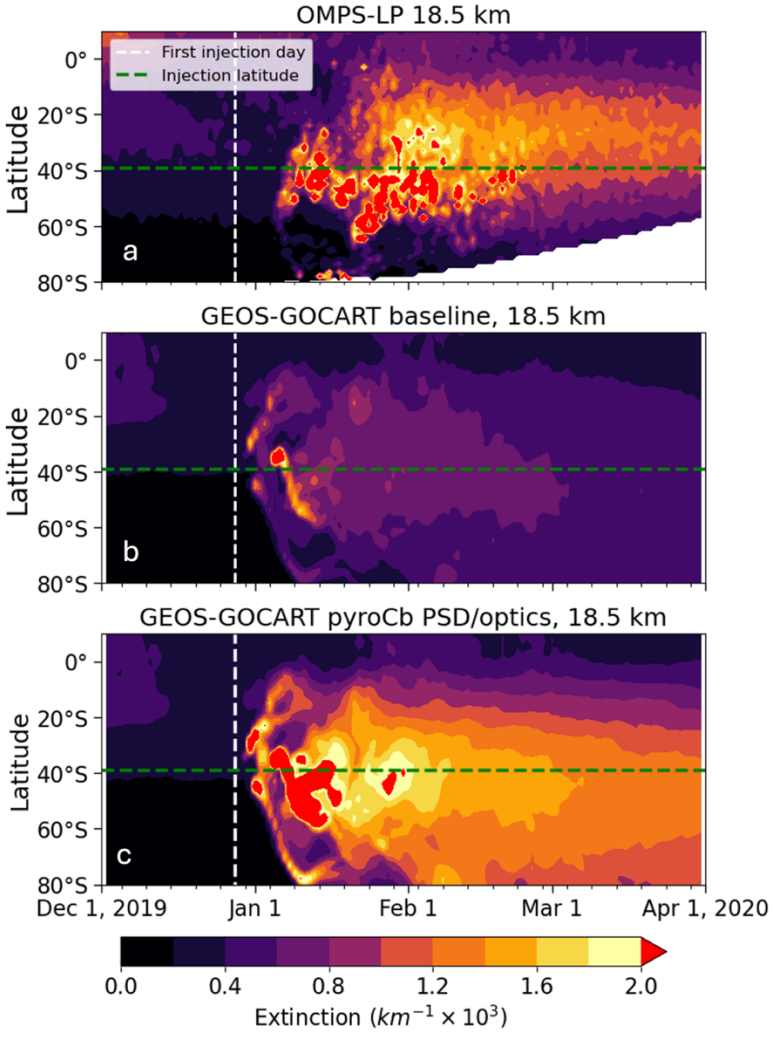

https://doi.org/10.5194/egusphere-2026-5642
Preprint. Discussion started: 25 September 2026

Figure 7. Zonal mean aerosol extinctions at 870 nm along the 18.5 km altitude surface from December 1, 2019, to April 1, 2020. (a) OMPS-LP observations, (b) the baseline GEOS configuration, and (c) the GEOS configuration utilizing the updated pyroCb PSD/optics. The vertical dashed white line marks the onset of the initial pyroCb injections, and the horizontal dashed green line denotes the injection latitude (39°S). Blank regions at high southern latitudes in (a) indicate missing OMPS-LP retrievals during polar night.

3.4 Impacts on Radiative Heating and Surface Area for Heterogeneous Chemistry

The updated pyroCb PSD/optics alter the aerosol radiative forcing and subsequent thermodynamic evolution of the plume. While shifting to a larger particle size successfully increases the bulk extinction (due to higher MEE), it also inherently enhances the bulk aerosol absorption, which is the primary driver of shortwave diabatic heating within the plume. The consequence of this is evident when evaluating an intermediate sensitivity configuration where only the PSD is updated (Fig. S3b). In this "PSD only" scenario, the unscaled absorption potential drives excessive diabatic heating, creating exaggerated vertical buoyancy that prematurely lofts the plume well above the SAGE-III observed extinction peak.

To compensate for this and maintain realistic vertical transport, we explicitly constrained the organic aerosol/brown carbon absorption based on ORACLES observations (Das et al., 2024). This combined approach, which updates both the size distribution and the refractive absorption, yields a more scattering plume. As shown in Fig. S4a, the simulated Single Scattering Albedo (SSA) at 532 nm within the plume core varies between 0.83–0.89 in the baseline model compared to 0.90–0.94 with the new optics over the first month after injection, a difference expected to be even larger in the near-UV. Consequently, the finalized pyroCb PSD/optics configuration successfully curbed the excessive lofting, bringing the simulated vertical transport into excellent agreement with SAGE-III observations (Fig. S3c).

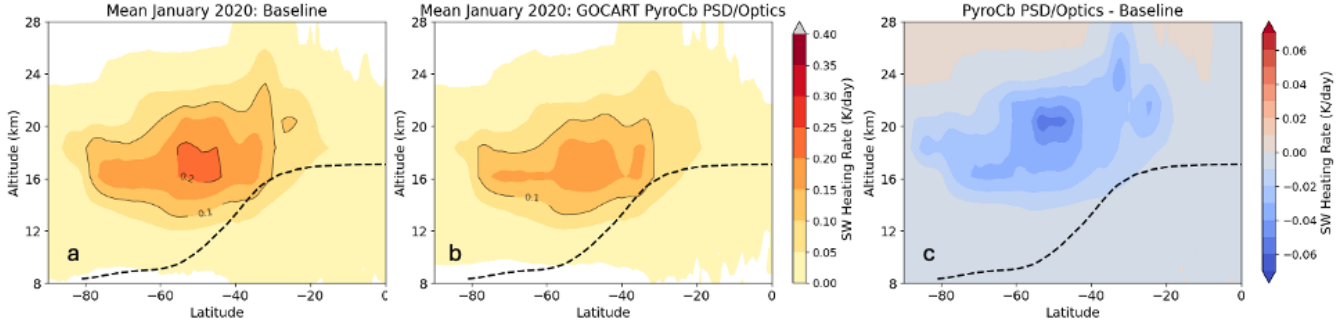

Figure 8. Zonal mean Shortwave (SW) Heating Rates (K day^{-1}) averaged over January 2020 for (a) the baseline GEOS configuration and (b) the updated pyroCb PSD/optics configuration. (c) The difference in SW heating rates (pyroCb PSD/optics minus baseline). The dashed black line denotes the tropopause height. Black contours in (a) and (b) indicate intervals of 0.1 K day^{-1}.

Figure 8 illustrates the resulting zonal mean shortwave (SW) heating rates for January 2020. Utilizing the pyroCb PSD/optics (Fig. 8b), stratospheric SW heating reaches approximately 0.15 to 0.20 K day^{-1} in the plume core. These values fall within the range of recent literature estimates for the ANY event. Earlier observationally constrained studies estimated localized heating rates of 0.2 to 0.4 K day^{-1} (Khaykin et al., 2020; Yu et al., 2021). However, our broad temporal and zonal monthly means

https://doi.org/10.5194/egusphere-2026-5642
Preprint. Discussion started: 25 September 2026

naturally smooth out these higher instantaneous rates found within highly concentrated smoke vortices. Consistent with this averaging effect, a more recent modeling study by Chen et al. (2026) reported lower peak zonal mean heating rates of ~0.12 K day^{-1}. Thus, our simulated heating rate of 0.15 to 0.20 K day^{-1} serves as an intermediate value. In contrast, the baseline model's lower SSA drives higher initial diabatic heating, peaking between 0.20 to 0.25 K day^{-1} (Fig. 8a). As shown in the difference plot (Fig. 8c), the baseline model produces approximately 20–25% (0.04 to 0.06 K day^{-1}) greater stratospheric SW heating overall. Because this elevated heating causes the baseline model to loft slightly more aerosol mass to higher altitudes, these heating differences are most pronounced above the primary plume core.

This variation in buoyancy and vertical mass distribution also leads to subtle differences in the large-scale horizontal transport. For example, tracking the geographic trajectory of the plume core (Fig. S4d) reveals a distinct dynamic divergence between the two configurations south of Chile, between days 15 and 20, the specific region where a highly distinct, self-maintaining smoke vortex (also called a SWIRL) was documented by Ohneiser et al. (2022). However, when evaluating these transport variations against SAGE-III or OMPS-LP satellite retrievals, it remains difficult to definitively establish which configuration yields the more accurate spatial mass distribution. Since satellite instruments retrieve optical extinction rather than direct aerosol mass, any discrepancy between the model and the observations can be driven by either (a) actual errors in the simulated physical mass distribution, or (b) erroneous MEE assumptions. Nonetheless, updating the baseline MEE to reflect observationally constrained particle sizes ensures that the resulting radiative and optical calculations are microphysically consistent.

While updating the particle size distribution moderates the diabatic heating and plume transport, it simultaneously drives a massive reduction in the available Surface Area Density (SAD) for heterogeneous chemistry because for a given total aerosol mass, SAD is inversely proportional to particle size.

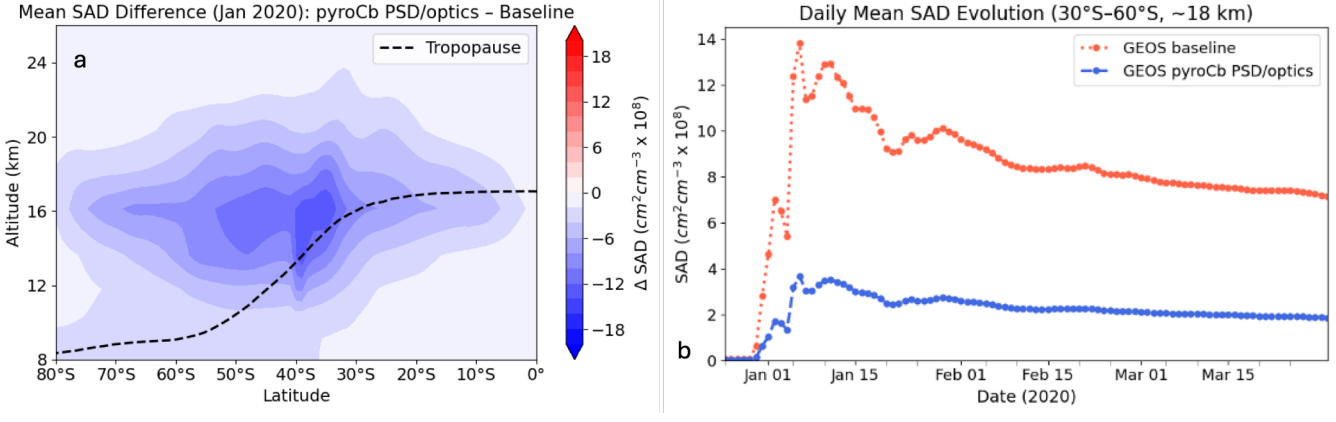

Figure 9. a) Zonal mean difference in Surface Area Density (SAD, cm² cm⁻³ × 10⁸) between the updated pyroCb PSD/optics configuration and the baseline GEOS configuration, averaged over January 2020. The dashed black line denotes the tropopause. (b) Daily mean SAD evolution from December 25, 2019, to March 31, 2020, averaged over the 30°S–60°S latitude band at the ~18 km altitude level for the baseline (dotted red line with markers) and pyroCb PSD/optics (dashed blue line with markers) configurations.

https://doi.org/10.5194/egusphere-2026-5642
Preprint. Discussion started: 25 September 2026

Figure 9 illustrates both the spatial discrepancy and the temporal evolution of SAD between the two model configurations. As shown in the monthly mean difference for January 2020 (Fig. 9a), shifting to a larger particle size distribution result in a substantial reduction in reactive surface area (reaching -12 to -18 × 10^{-8} cm^2 cm^{-3}) that is perfectly co-located with the core of the spreading smoke plume. Tracking the daily mean SAD at the ~18 km altitude level (Fig. 9b) further highlights the magnitude of this divergence: while both configurations simulate a sharp increase following the primary injections, the baseline fine-mode assumption generates a prolonged peak that is more than a factor of three larger than that of the updated pyroCb PSD/optics. Although direct observations of SAD are unavailable to definitively validate the absolute magnitudes of either simulation, this large relative difference underscores how heavily modelled heterogeneous chemical reaction rates depend on fundamental microphysical assumptions. The cascading impacts of this surface area discrepancy on stratospheric composition, especially for the repartitioning of inorganic chlorine, NO_x depletion, and subsequent ozone depletion, are being explicitly explored in a subsequent study.

4 Summary and Conclusions

Global Earth System Models (ESMs) rely on computationally efficient bulk aerosol parameterisations that are fundamentally designed and tuned for typical tropospheric smoke. However, the 2019/2020 Australian New Year (ANY) pyroCb events provided a stark reminder that stratospheric pyroCb-emitted particles are vastly different from standard tropospheric aerosols. Applying default finer-mode, non-evolving tropospheric assumptions to these extreme stratospheric injections compromises a model's ability to accurately capture the plume's optical thickness, dynamic transport, and chemical reactivity. In lieu of comprehensive direct observations of these unique pyroCb particles, this study demonstrates how sophisticated sectional microphysics models can be leveraged to inform and update bulk parameterisations, bringing efficient global climate simulations closer to reality.

In this study, we dynamically simulated the microphysical aging of the ANY pyroCb plume using the CARMA sectional module within the NASA GEOS framework. We found that the intense concentration of fresh smoke rapidly drives coagulation, stabilizing the stratospheric aerosol effective radius at ~0.30 µm within the first few weeks, which is a massive shift compared to standard tropospheric baseline assumptions (R_{eff} = 0.09 µm), but perfectly in line with recent in-situ and multi-wavelength lidar observations.

To translate this physical reality to the computationally efficient GOCART-2G bulk aerosol scheme, we utilised offline Mie theory to design an observationally constrained "pyroCb PSD/optics" configuration. We determined that accurately reproducing the high Mass Extinction Efficiency (MEE) of the aged smoke requires not only a larger effective radius (R_{eff} = 0.30 µm) but also a narrower size distribution (σ = 1.2). Because shifting to a larger particle size inherently increases both bulk scattering and bulk absorption, we explicitly adjusted the organic aerosol absorption to yield a more scattering plume. While direct in-situ or lidar measurements of Single Scattering Albedo (SSA) for the mature pyroCb plumes are lacking, we

https://doi.org/10.5194/egusphere-2026-5642
Preprint. Discussion started: 25 September 2026

successfully constrained this absorption potential based on our prior modelling of the 2017 British Columbia pyroCb events (Das et al., 2021) and tropospheric smoke over south-east Atlantic region (Das et al., 2024). We note that while these constraints vastly improve model performance, there remains a critical need for more direct observational campaigns targeting the microphysical and optical properties of both, fresh and aged pyroCb smoke to further refine these parameters. Implementing this modified configuration in GEOS yielded substantial improvements across major physical and optical metrics:

1. **Optical Fidelity:** The updated configuration successfully reproduced the high aerosol extinction magnitudes and the characteristic drop in Ångström Exponent (~1.4–1.5) observed by SAGE-III/ISS at the smoke-influenced stratospheric layers compared to the background state (~2–2.5), whereas the baseline model remained optically muted and erroneously reflected background stratospheric particle sizes.

2. **Radiative Heating and Plume Transport:** Explicitly moderating the absorption potential of the larger particles was critical to avoid excessive heating and unrealistic vertical buoyancy. The finalized configuration yielded shortwave heating rates (0.15–0.20 K day^{-1}) in agreement with recent observational and modelling literature, which successfully prevented premature lofting and enabled the model to accurately capture both the vertical plume placement observed by SAGE-III and the sustained equatorward spread and longevity tracked by OMPS-LP across peak smoke altitudes.

3. **Reactive Surface Area:** Because larger particles possess less surface area per unit mass, the updated microphysics reduced the total available aerosol Surface Area Density (SAD) by more than a factor of three compared to the baseline model.

This study provides a critical bridge between sophisticated sectional aerosol microphysics models and computationally efficient bulk aerosol schemes. By demonstrating that a simplified but observationally constrained particle size assumption can vastly improve simulations of aerosol optics and transport, we offer a pragmatic pathway for ESMs to better represent extreme wildfire events. The key implication is twofold: first, realistic plume transport and radiative forcing can be achieved without computationally prohibitive schemes. Second, we reveal that the surface area available for heterogeneous chemistry is more than three times smaller than default assumptions would suggest. This latter finding could have substantial consequences for stratospheric chemistry, requiring a reassessment of the magnitude of wildfire smoke's impact on key stratospheric chemical cycles, such as inorganic chlorine and NO_x, and subsequent ozone depletion. Therefore, this work provides a more observationally-constrained and physically-consistent global model configuration essential for accurately quantifying the full climate and chemical impacts of large pyrocumulonimbus injections on the stratosphere.

Code availability. The GEOS Earth System Model, including GOCART-2G and CARMA source code and the instructions for model build are available at https:// github.com/GEOS-ESM/GEOSgcm/ (last access: 14 July 2025) and https://doi.org/10.5281/zenodo.10927491 (Colarco, 2024).

Data availability. The processed model output datasets, in NetCDF format, required to reproduce the figures and analyses presented in this study are available for peer review at [Zenodo: Link for Peer Review]. Upon acceptance, the data will be

https://doi.org/10.5194/egusphere-2026-5642
Preprint. Discussion started: 25 September 2026

published on Zenodo with the permanent DOI:10.5281/zenodo.22680076. The observational datasets used for model evaluation and boundary conditions are publicly available from the following sources: the **SAGE-III/ISS** Version 5.3 Level 2 aerosol extinction data are available from the NASA Langley Atmospheric Science Data Center (ASDC) DAAC at https://doi.org/10.5067/ISS/SAGEIII/SOLAR_BINARY_L2-V5.3 (SAGE Science Team, 2023). The **OMPS-LP** standard Version 2.5 aerosol extinction retrieval product is available through the NASA Goddard Earth Sciences Data and Information Services Center (GES DISC) at https://doi.org/10.5067/6X1B487WO4W1 (Taha, 2025). The specific cloud-unfiltered OMPS-LP data utilized to preserve the dense smoke signals in this study are included alongside the modeling data in the aforementioned Zenodo repository. **Meteorological Fields:** The assimilated meteorological fields used to constrain the GEOS simulations were provided by the near-real-time GEOS-FP system (version f522), accessible via the NASA Global Modeling and Assimilation Office (GMAO) at https://gmao.gsfc.nasa.gov/weather-analysis-prediction/.

Author contributions. SD and PRC conceptualized the modeling and analysis approach and wrote the manuscript. PRC performed the GEOS-GOCART2G model simulations and PC performed the GEOS-CARMA simulations. PRC, SS and SD implemented the code developments within GMI chemistry module and its coupling with the GOCART-2G aerosol module. LO provided guidance on the modeling approach and continuous support throughout the study. GT provided the cloud-unfiltered version of OMPS version 2.5 aerosol product. All authors contributed to the editing of the manuscript.

Competing interests. The authors declare that they have no conflict of interest.

Acknowledgements. This work was supported by NASA ROSES ACMAP-22 grant 80NSSC23K0922.We would like to acknowledge the NASA Earth Science Division and GEOS model developmental efforts at GMAO for their support. The computing resources supporting this work were provided by the NASA High-End Computing (HEC) Program through the NASA Center for Climate Simulation (NCCS) at the Goddard Space Flight Center.

5 References

Case, P., Colarco, P. R., Toon, B., Aquila, V. and Keller, C. A.: Interactive Stratospheric Aerosol Microphysics-Chemistry Simulations of the 1991 Pinatubo Volcanic Aerosols With Newly Coupled Sectional Aerosol and Stratosphere-Troposphere Chemistry Modules in the NASA GEOS Chemistry-Climate Model (CCM), J. Adv. Model. Earth Syst., 15(8), doi:10.1029/2022MS003147, 2023.

Case, P. A., Colarco, P. R., Toon, O. B. and Newman, P. A.: Simulating the Volcanic Sulfate Aerosols From the 1991 Eruption of Cerro Hudson and Their Impact on the 1991 Ozone Hole, Geophys. Res. Lett., 51(5), doi:10.1029/2023GL106619, 2024.

Chen, X., Wang, J., Peterson, D. A., Li, Y., Julstrom, W., Keutsch, F. and Dykema, J.: Large Particle Size and Thick Coating Influence Pyrocumulonimbus Smoke Radiative Forcing and Stratospheric Warming: Insights from the 2019-2020 Australian Megafires, ESS Open Arch., 2026(0413), doi:10.22541/essoar.15001964/v1, 2026.

Chin, M., Ginoux, P., Kinne, S., Torres, O., Holben, B. N., Duncan, B. N., Martin, R. V., Logan, J. A., Higurashi, A. and Nakajima, T.: Tropospheric aerosol optical thickness from the GOCART model and comparisons with satellite and sun photometer measurements, J. Atmos. Sci., 59(3 PT 1), doi:10.1175/1520-0469(2002)059<0461:taotft>2.0.co;2, 2002.

Cisewski, M., Zawodny, J., Gasbarre, J., Eckman, R., Topiwala, N., Rodriguez-Alvarez, O., Cheek, D., and Hall, S.: The Stratospheric Aerosol and Gas Experiment (SAGE III) on the International Space Station (ISS) Mission, in: SPIE Remote Sensing, edited by Meynart, R., Neeck, S. P., and Shimoda, H., p. 924107, Amsterdam, Netherlands,

https://doi.org/10.5194/egusphere-2026-5642
Preprint. Discussion started: 25 September 2026

https://doi.org/10.1117/12.2073131, 2014.

Colarco, P., Da Silva, A., Chin, M. and Diehl, T.: Online simulations of global aerosol distributions in the NASA GEOS-4 model and comparisons to satellite and ground-based aerosol optical depth, J. Geophys. Res. Atmos., 115(14), doi:10.1029/2009JD012820, 2010.

Colarco, P. R., Nowottnick, E. P., Randles, C. A., Yi, B., Yang, P., Kim, K. M., Smith, J. A. and Bardeen, C. G.: Impact of radiatively interactive dust aerosols in the NASA GEOS-5 climate model: Sensitivity to dust particle shape and refractive index, J. Geophys. Res., 119(2), doi:10.1002/2013JD020046, 2014.

Colarco, P. R., Gassó, S., Ahn, C., Buchard, V., Dasilva, A. M. and Torres, O.: Simulation of the Ozone Monitoring Instrument aerosol index using the NASA Goddard Earth Observing System aerosol reanalysis products, Atmos. Meas. Tech., 10(11), doi:10.5194/amt-10-4121-2017, 2017.

Colarco, P.: GEOS Earth System Model, Zenodo [code], https://doi.org/10.5281/zenodo.10927491, 2024.

Collow, A. B., Colarco, P. R., Da Silva, A. M., Buchard, V., Bian, H., Chin, M., Das, S., Govindaraju, R., Kim, D. and Aquila, V.: Benchmarking GOCART-2G in the Goddard Earth Observing System (GEOS), Geosci. Model Dev., 17(3), doi:10.5194/gmd-17-1443-2024, 2024.

Das, S., Colarco, P. R., Oman, L. D., Taha, G. and Torres, O.: The long-term transport and radiative impacts of the 2017 British Columbia pyrocumulonimbus smoke aerosols in the stratosphere, Atmos. Chem. Phys., 21(15), doi:10.5194/acp-21-12069-2021, 2021.

Das, S., Colarco, P. R., Bian, H. and Gassó, S.: Improved simulations of biomass burning aerosol optical properties and lifetimes in the NASA GEOS Model during the ORACLES-I campaign, Atmos. Chem. Phys., 24(7), doi:10.5194/acp-24-4421-2024, 2024.

Flynn, L., Long, C., Wu, X., Evans, R., Beck, C. T., Petropavlovskikh, I., McConville, G., Yu, W., Zhang, Z., Niu, J., Beach, E., Hao, Y., Pan, C., Sen, B., Novicki, M., Zhou, S. and Seftor, C.: Performance of the ozone mapping and profiler suite (OMPS) products, J. Geophys. Res., 119(10), doi:10.1002/2013JD020467, 2014.

Fromm, M., Lindsey, D. T., Servranckx, R., Yue, G., Trickl, T., Sica, R., Doucet, P. and Godin-Beekmann, S.: The untold story of pyrocumulonimbus, Bull. Am. Meteorol. Soc., 91(9), doi:10.1175/2010BAMS3004.1, 2010.

Hodzic, A. and Jimenez, J. L.: Modeling anthropogenically controlled secondary organic aerosols in a megacity: A simplified framework for global and climate models, Geosci. Model Dev., 4(4), doi:10.5194/gmd-4-901-2011, 2011.

Kablick, G. P., Allen, D. R., Fromm, M. D. and Nedoluha, G. E.: Australian PyroCb Smoke Generates Synoptic-Scale Stratospheric Anticyclones, Geophys. Res. Lett., 47(13), doi:10.1029/2020GL088101, 2020.

Katich, J. M., Apel, E. C., Bourgeois, I., Brock, C. A., Bui, T. P., Campuzano-Jost, P., Commane, R., Daube, B., Dollner, M., Fromm, M., Froyd, K. D., Hills, A. J., Hornbrook, R. S., Jimenez, J. L., Kupc, A., Lamb, K. D., McKain, K., Moore, F., Murphy, D. M., Nault, B. A., Peischl, J., Perring, A. E., Peterson, D. A., Ray, E. A., Rosenlof, K. H., Ryerson, T., Schill, G. P., Schroder, J. C., Weinzierl, B., Thompson, C., Williamson, C. J., Wofsy, S. C., Yu, P. and Schwarz, J. P.: Pyrocumulonimbus affect average stratospheric aerosol composition, Science (80-.)., 379(6634),

https://doi.org/10.5194/egusphere-2026-5642
Preprint. Discussion started: 25 September 2026

doi:10.1126/science.add3101, 2023.

Khaykin, S., Legras, B., Bucci, S., Sellitto, P., Isaksen, L., Tencé, F., Bekki, S., Bourassa, A., Rieger, L., Zawada, D., Jumelet, J. and Godin-Beekmann, S.: The 2019/20 Australian wildfires generated a persistent smoke-charged vortex rising up to 35 km altitude, Commun. Earth Environ., 1(1), doi:10.1038/s43247-020-00022-5, 2020.

Kim, P. S., Jacob, D. J., Fisher, J. A., Travis, K., Yu, K., Zhu, L., Yantosca, R. M., Sulprizio, M. P., Jimenez, J. L., Campuzano-Jost, P., Froyd, K. D., Liao, J., Hair, J. W., Fenn, M. A., Butler, C. F., Wagner, N. L., Gordon, T. D., Welti, A., Wennberg, P. O., Crounse, J. D., St. Clair, J. M., Teng, A. P., Millet, D. B., Schwarz, J. P., Markovic, M. Z. and Perring, A. E.: Sources, seasonality, and trends of southeast US aerosol: An integrated analysis of surface, aircraft, and satellite observations with the GEOS-Chem chemical transport model, Atmos. Chem. Phys., 15(18), doi:10.5194/acp-15-10411-2015, 2015.

Li, Y., Dykema, J. A., Peterson, D. A., Feng, X., Shen, X., June, N. A., Fromm, M. D., McHardy, T. M., Jacquot, J. L., Pittman, J. V., Daube, B. C., Wofsy, S. C., Dean-Day, J., Rapp, A. D., Bowman, K. P., Cziczo, D. J., Mickley, L. J., Pierce, J. R. and Keutsch, F. N.: Enhanced radiative cooling by large aerosol particles from wildfire-driven thunderstorms, Sci. Adv. , 11(50), doi:10.1126/sciadv.adw6526, 2025.

Molod, A., Takacs, L., Suarez, M. and Bacmeister, J.: Development of the GEOS-5 atmospheric general circulation model: Evolution from MERRA to MERRA2, Geosci. Model Dev., 8(5), doi:10.5194/gmd-8-1339-2015, 2015.

Murphy, D. M., Froyd, K. D., Bourgeois, I., Brock, C. A., Kupc, A., Peischl, J., Schill, G. P., Thompson, C. R., Williamson, C. J. and Yu, P.: Radiative and chemical implications of the size and composition of aerosol particles in the existing or modified global stratosphere, Atmos. Chem. Phys., 21(11), doi:10.5194/acp-21-8915-2021, 2021.

Ohneiser, K., Ansmann, A., Kaifler, B., Chudnovsky, A., Barja, B., Knopf, D. A., Kaifler, N., Baars, H., Seifert, P., Villanueva, D., Jimenez, C., Radenz, M., Engelmann, R., Veselovskii, I. and Zamorano, F.: Australian wildfire smoke in the stratosphere: The decay phase in 2020/2021 and impact on ozone depletion, Atmos. Chem. Phys., 22(11), doi:10.5194/acp-22-7417-2022, 2022.

Peterson, D. A., Campbell, J. R., Hyer, E. J., Fromm, M. D., Kablick, G. P., Cossuth, J. H. and DeLand, M. T.: Wildfire-driven thunderstorms cause a volcano-like stratospheric injection of smoke, npj Clim. Atmos. Sci., 1(1), doi:10.1038/s41612-018-0039-3, 2018.

Peterson, D. A., Fromm, M. D., McRae, R. H. D., Campbell, J. R., Hyer, E. J., Taha, G., Camacho, C. P., Kablick, G. P., Schmidt, C. C. and DeLand, M. T.: Australia's Black Summer pyrocumulonimbus super outbreak reveals potential for increasingly extreme stratospheric smoke events, npj Clim. Atmos. Sci., 4(1), doi:10.1038/s41612-021-00192-9, 2021.

Putman, W. M. and Lin, S. J.: Finite-volume transport on various cubed-sphere grids, J. Comput. Phys., 227(1), doi:10.1016/j.jcp.2007.07.022, 2007.

Putman, W. M. and Suarez, M.: Cloud-system resolving simulations with the NASA Goddard Earth Observing System global atmospheric model (GEOS-5), Geophys. Res. Lett., 38(16), doi:10.1029/2011GL048438, 2011.

Redemann, J., Wood, R., Zuidema, P., Doherty, S. J., Luna, B., LeBlanc, S. E., Diamond, M. S., Shinozuka, Y., Chang, I. Y., Ueyama, R., Pfister, L., Ryoo, J. M., Dobracki, A. N., da Silva, A. M., Longo, K. M., Kacenelenbogen, M. S., Flynn, C. J.,

https://doi.org/10.5194/egusphere-2026-5642
Preprint. Discussion started: 25 September 2026

Pistone, K., Knox, N. M., Piketh, S. J., Haywood, J. M., Formenti, P., Mallet, M., Stier, P., Ackerman, A. S., Bauer, S. E., Fridlind, A. M., Carmichael, G. R., Saide, P. E., Ferrada, G. A., Howell, S. G., Freitag, S., Cairns, B., Holben, B. N., Knobelspiesse, K. D., Tanelli, S., L'Ecuyer, T. S., Dzambo, A. M., Sy, O. O., McFarquhar, G. M., Poellot, M. R., Gupta, S., O'Brien, J. R., Nenes, A., Kacarab, M., Wong, J. P. S., Small-Griswold, J. D., Thornhill, K. L., Noone, D., Podolske, J. R., Sebastian Schmidt, K., Pilewskie, P., Chen, H., Cochrane, S. P., Sedlacek, A. J., Lang, T. J., Stith, E., Segal-Rozenhaimer, M., Ferrare, R. A., Burton, S. P., Hostetler, C. A., Diner, D. J., Seidel, F. C., Platnick, S. E., Myers, J. S., Meyer, K. G., Spangenberg, D. A., Maring, H. and Gao, L.: An overview of the ORACLES (ObseRvations of aerosols above CLouds and their intEractionS) project: Aerosol-cloud-radiation interactions in the southeast Atlantic basin, Atmos. Chem. Phys., 21(3), doi:10.5194/acp-21-1507-2021, 2021.

Rienecker, M. M., Suarez, M. J., Todling, R., Bacmeister, J., Takacs, L., Liu, H.-C., Gu, W., Sienkiewicz, M., Koster, R. D., Gelaro, R., Stajner, I., and Nielsen, J. E.: The GEOS-5 Data Assimilation System – Documentation of Versions 5.0.1, 5.1.0, and 5.2.0, Technical Report Series on Global Modeling and Data Assimilation, NASA/TM-2008-104606, Vol. 27, 118 pp., available at: https://gmao.gsfc.nasa.gov/pubs/docs/GEOS5_104606-Vol27.pdf (accessed 24 November 2025), 2008.

SAGE Science Team: SAGE III/ISS L2 Monthly Aerosol Product (netCDF) V011, NASA Langley Atmospheric Science Data Center Distributed Active Archive Center [data set], https://doi.org/10.5067/ISS/SAGEIII/AEROSOL_NetCDF4_L2-V1.1 (accessed 26 March 2025), 2023.

Santee, M. L., Lambert, A., Manney, G. L., Livesey, N. J., Froidevaux, L., Neu, J. L., Schwartz, M. J., Millán, L. F., Werner, F., Read, W. G., Park, M., Fuller, R. A. and Ward, B. M.: Prolonged and Pervasive Perturbations in the Composition of the Southern Hemisphere Midlatitude Lower Stratosphere From the Australian New Year's Fires, Geophys. Res. Lett., 49(4), doi:10.1029/2021GL096270, 2022.

Schwartz, M. J., Santee, M. L., Pumphrey, H. C., Manney, G. L., Lambert, A., Livesey, N. J., Millán, L., Neu, J. L., Read, W. G. and Werner, F.: Australian New Year's PyroCb Impact on Stratospheric Composition, Geophys. Res. Lett., 47(24), doi:10.1029/2020GL090831, 2020.

Sellitto, P., Belhadji, R., Cuesta, J., Podglajen, A. and Legras, B.: Radiative impacts of the Australian bushfires 2019-2020 - Part 2: Large-scale and in-vortex radiative heating, Atmos. Chem. Phys., 23(24), doi:10.5194/acp-23-15523-2023, 2023.

Solomon, S., Dube, K., Stone, K., Yu, P., Kinnison, D., Toon, O. B., Strahan, S. E., Rosenlof, K. H., Portmann, R., Davis, S., Randel, W., Bernath, P., Boone, C., Bardeen, C. G., Bourassa, A., Zawada, D. and Degenstein, D.: On the stratospheric chemistry of midlatitude wildfire smoke, Proc. Natl. Acad. Sci. U. S. A., 119(10), doi:10.1073/pnas.2117325119, 2022.

Solomon, S., Stone, K., Yu, P., Murphy, D. M., Kinnison, D., Ravishankara, A. R. and Wang, P.: Chlorine activation and enhanced ozone depletion induced by wildfire aerosol, Nature, 615(7951), doi:10.1038/s41586-022-05683-0, 2023.

Strahan, S. E., Smale, D., Solomon, S., Taha, G., Damon, M. R., Steenrod, S. D., Jones, N., Liley, B., Querel, R. and Robinson, J.: Unexpected Repartitioning of Stratospheric Inorganic Chlorine After the 2020 Australian Wildfires, Geophys. Res. Lett., 49(14), doi:10.1029/2022GL098290, 2022.

Taha, G., Loughman, R., Zhu, T., Thomason, L., Kar, J., Rieger, L. and Bourassa, A.: OMPS LP Version 2.0 multi-wavelength

https://doi.org/10.5194/egusphere-2026-5642
Preprint. Discussion started: 25 September 2026

aerosol extinction coefficient retrieval algorithm, Atmos. Meas. Tech., 14(2), doi:10.5194/amt-14-1015-2021, 2021.

Taha, G.: OMPS-NPP L2 LP Aerosol Extinction Vertical Profile swath daily 3slit V2.5, NASA Goddard Earth Sciences Data and Information Services Center (GES DISC) [data set], https://doi.org/10.5067/6X1B487WO4W1(accessed 15 September 2025), 2025.

Thomason, L. W. and Taha, G.: SAGE III aerosol extinction measurements: Initial results, Geophys. Res. Lett., 30(12), doi:10.1029/2003GL017317, 2003.

Thomason, L. W., Moore, J. R., Pitts, M. C., Zawodny, J. M. and Chiou, E. W.: An evaluation of the SAGE~III version 4 aerosol extinction coefficient and water vapor data products, Atmos. Chem. Phys., 10(5), doi:10.5194/acp-10-2159-2010, 2010.

Toon, O. B., Turco, R. P., Westphal, D., Malone, R. and Liu, M. S.: A multidimensional model for aerosols: description of computational analogs, J. Atmos. Sci., 45(15), doi:10.1175/1520-0469(1988)045<2123:ammfad>2.0.co;2, 1988.

Yu, P., Davis, S. M., Toon, O. B., Portmann, R. W., Bardeen, C. G., Barnes, J. E., Telg, H., Maloney, C. and Rosenlof, K. H.: Persistent Stratospheric Warming Due to 2019–2020 Australian Wildfire Smoke, Geophys. Res. Lett., 48(7), doi:10.1029/2021GL092609, 2021.